ACS APPLIED MATERIALS & INTERFACES

Research Article

www.acsami.org

Two Similar Near-Infrared (IR) Absorbing Benzannulated Aza-BODIPY Dyes as Near-IR Sensitizers for Ternary Solar Cells

Jie Min,*[,†] Tayebeh Ameri,[†] Roland Gresser,[§] Melanie Lorenz-Rothe,[§] Derya Baran,[†] Anna Troeger,[⊥] Vito Sgobba,[⊥] Karl Leo,[§] Moritz Riede,[§] Dirk M. Guldi,[⊥] and Christoph J. Brabec[†,‡]

[†]Institute of Materials for Electronics and Energy Technology (I-MEET), Friedrich-Alexander-University Erlangen-Nuremberg, Martensstraße 7, 91058 Erlangen, Germany

[‡]Bavarian Center for Applied Energy Research (ZAE Bayern), Haberstraße 2a, 91058 Erlangen, Germany

[§]Institut für Angewandte Photophysik, Technische Universität Dresden, George-Bähr-Straße 1, 01069 Dresden, Germany

[⊥]Department of Chemistry and Pharmacy & Interdisciplinary Center for Molecular Materials, University of Erlangen-Nuremberg, Egerlandstrasse 3, 91058 Erlangen, Germany

Supporting Information

ABSTRACT: Ternary composite inverted organic solar cells based on poly(3-hexylthiophen-2,5-diyl) (P3HT) and phenyl-C_{61}-butyric acid methyl ester (PCBM) blended with two different near-infrared absorbing benzannulated aza-BODIPY dyes, difluoro-bora-bis-(1-phenyl-indoyl)-azamethine (**1**) or difluoro-bora-bis-(1-(5-methylthiophen)-indoyl)-azamethine (**2**), were constructed and characterized. The amount of these two aza-BODIPY dyes, within the P3HT and PCBM matrix, was systematically varied, and the characteristics of the respective devices were recorded. Although the addition of both aza-BODIPY dyes enhanced the absorption of the blends, only the addition of **1** improved the overall power conversion efficiency (PCE) in the near-infrared (IR) region. The present work paves the way for the integration of near-infrared absorbing aza-BODIPY derivatives as sensitizers in ternary composite solar cells.

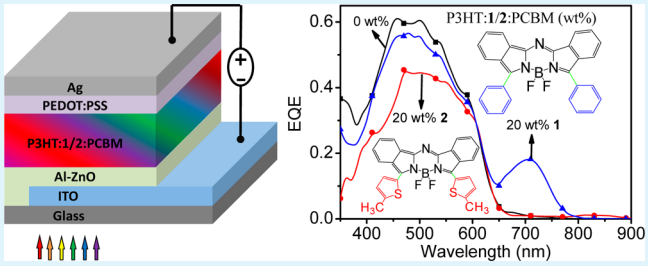

KEYWORDS: *inverted organic solar cells, aza-BODIPY dye, power conversion efficiency, near-IR absorbing, sensitizer, ternary composite solar cells*

1. INTRODUCTION

Bulk heterojunction (BHJ) solar cells based on polymer/fullerene blends have prompted significant interest as a promising technology for renewable energy owing to their potential advantages such as low cost, lightweight, and large-area fabrication on flexible substrates.[1−5] To date, promising power conversion efficiencies (PCEs) of ca. 9% were achieved in BHJ polymer solar cells (PSCs),[6,7] with room left for enhanced spectral sensitivity in the visible as well as in the near-infrared (IR) region.

In recent years, the most thoroughly studied materials for the active layer are blends of regioregular poly(3-hexylthiophen-2,5-diyl) (P3HT, Figure 1a) and [6,6]-phenyl-C_{61}-butyric acid methyl ester (PCBM, Figure 1a). Controlling the morphology in P3HT:PCBM solar cells has led to reproducible PCEs of around 4−5%.[8] Further PCE improvements are limited by: (i) the relatively high lying highest occupied molecular orbital (HOMO) energy level of P3HT (ca. −4.8 eV),[9] (ii) the not optimal overlap of P3HT absorption with the solar spectrum, and (iii) the too large open circuit voltage (V_{oc}) loss due to a significant offset in the P3HT/PCBM lowest unoccupied molecular orbitals (LUMOs).[10] Several methods have been pursued to overcome the aforementioned limitations and to achieve enhanced PCEs, including: implementing fullerene derivatives with higher LUMO as compared to PCBM,[11−13] employing conjugated polymers with lower HOMO and smaller band gap,[14−20] or integration of up-conversion materials into the interface layers.[21] The design of tandem structures, in which two or more cells are stacked, emerged as another effective method to enhance light harvesting. Nevertheless, in a tandem device, control and modification of the respective layer thickness and designing a full-functional intermediate layer are big challenges.[22−25] To this end, constructing ternary blend based solar cells by adding a suitable third component into the P3HT:PCBM matrix and processing the solution in a single-step is a promising alternative. For that, nanoparticles,[26,27] polymers,[28−30] and small molecules[31−35] have been recently integrated. Among small molecules, aza-BODIPY (4,4-difluoro-4-bora-3a,4a-diaza-s-indacene) dyes have attracted much interest owing to their high molecular extinction coefficients, photoluminescence quantum yield, and

Received: March 14, 2013
Accepted: May 31, 2013
Published: May 31, 2013

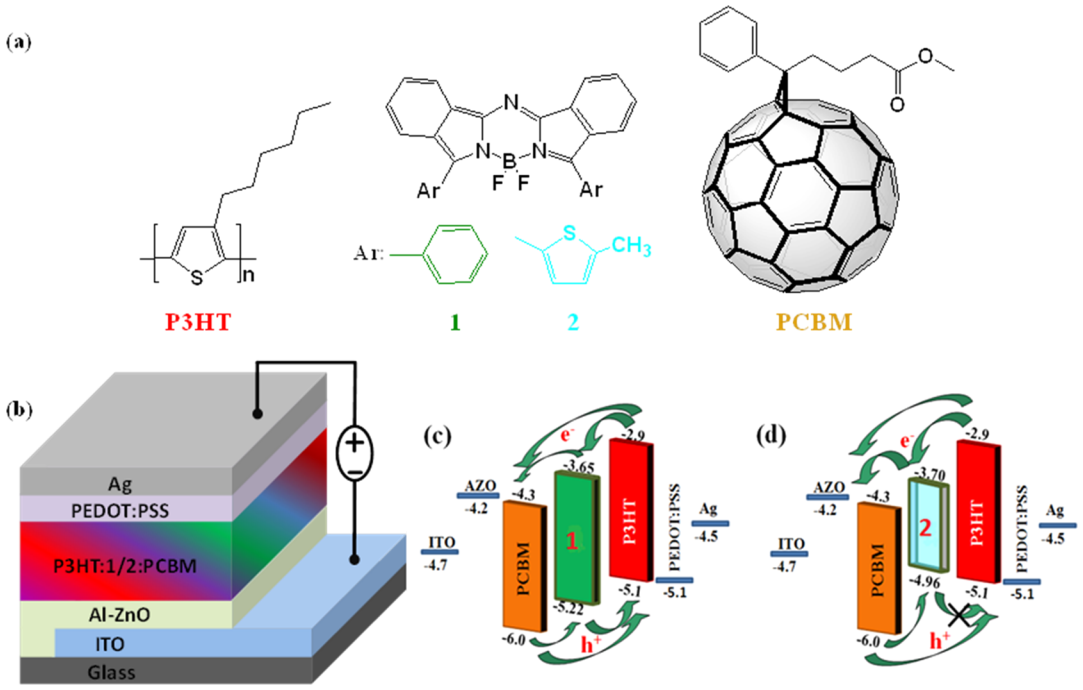

Figure 1. (a) Chemical structures of P3HT, **1**, **2**, and PCBM. (b) Schematic illustration of the P3HT:**1**:PCBM and P3HT:**2**:PCBM solar cell architecture. Schematic energy band diagram of (c) P3HT:**1**:PCBM and (d) P3HT:**2**:PCBM based solar cells.

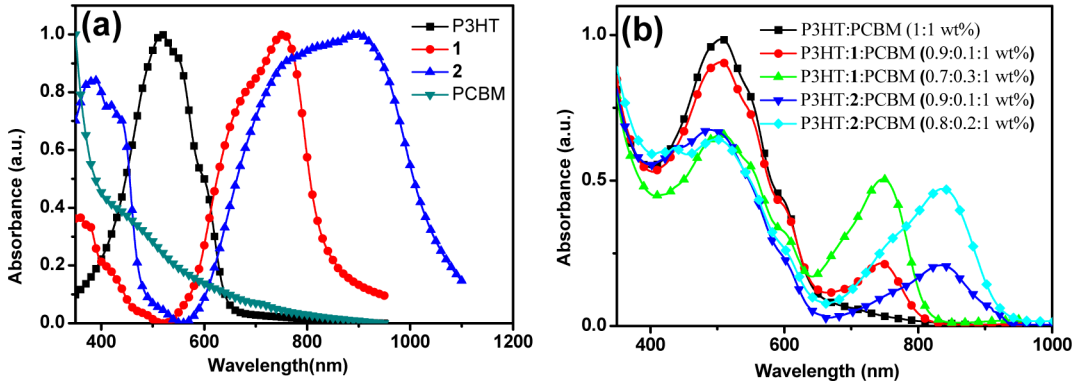

Figure 2. (a) Normalized absorption spectra of P3HT, **1**, **2**, and PCBM films. (b) Absorption spectra of thermally annealed P3HT:PCBM 1:1 wt % and P3HT:**1**:PCBM as well as P3HT:**2**:PCBM blend films at different **1** and **2** concentrations.

photostability.[33] They have been investigated as *p*-type or donor materials in solution-processed BHJ solar cells.[36−39]

In this work, we constructed and characterized two different BHJ solar cells (Figure 1b) based on P3HT:PCBM blends blended with two distinct aza-BODIPY dyes. To examine the relationship between the device performance and the energy levels of aza-BODIPY dyes, we utilized two near-IR absorbing benzannulated aza-BODIPY dyes: difluoro-bora-bis-(1-phenyl-indoyl)-azamethine (**1**) and difluoro-bora-bis-(1-(5-methylthiophen)-indoyl)-azamethine (**2**) (see Figure 1a). Their synthesis and characterization have been described elsewhere.[40] For a P3HT:**1**:PCBM ternary blend device, in comparison with P3HT:PCBM device, the EQE in the 700 nm regime increased up to 10% due to charge generation from the **1**, resulting in an overall short circuit current (J_{sc}) enhancement of 10% (from 7.03 to 7.76 mA/cm^2). Further enhancement of J_{sc} renders feasible for significantly thicker absorber layers. In contrast, the photovoltaic performances of P3HT:**2**:PCBM steadily decreased upon adding gradually increasing amounts of **2**, and no photocurrent contribution in the IR, where **2** absorbs, was observed. To shed more light onto the aforementioned trend, the photoactive materials are investigated by absorption spectroscopy, cyclic voltammetry (CV), spectroelectrochemistry (SEC), photoluminescence spectroscopy (PL), transient absorption spectroscopy (TAS), and atomic force microscopy (AFM).

2. RESULTS AND DISCUSSION

1 and **2** were synthesized according to the reported procedure[40] and have been implemented as near-IR sensitizers into the P3HT:PCBM host matrix to enhance the near-IR absorption and photogeneration as shown in Figure 2a. Figure 1b depicts the schematics of the inverted structure devices, featuring Al-doped ZnO (AZO) as the electron-transporting layer, PEDOT:PSS as the hole-transporting layer, and an air-stable high-work-function metal (Ag) as the anodic electrode for hole collection.

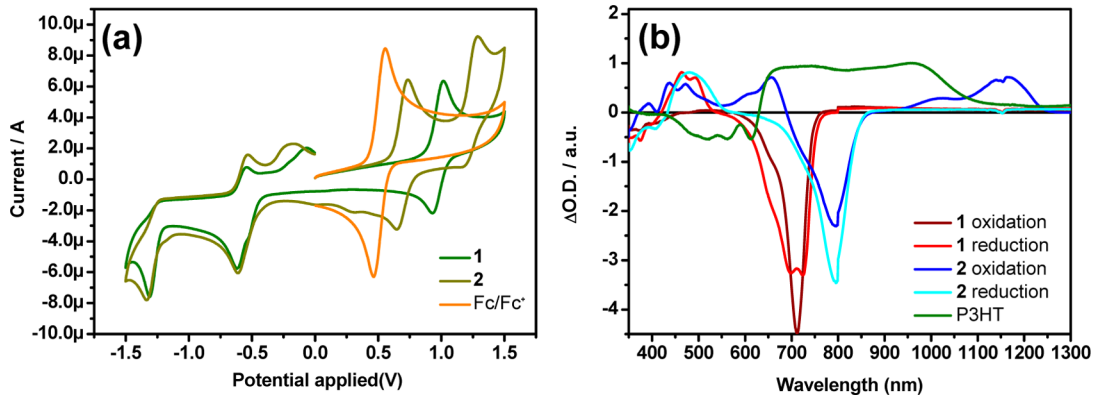

Figure 3. (a) Cyclic voltammograms of **1**, **2**, and ferrocene/ferrocenium (Fc/Fc^+) reference couple in dichloromethane at scan rate of 100 mVs^{-1}; working electrolyte: glassy carbon; counter electrode: platinum wire; pseudoreference electrode: silver wire; supporting electrolyte: 0.1 M tetrabutylammonium hexafluorophosphate. (b) Differential absorption spectrum of **1** in acetonitrile upon spectroelectrochemical oxidation at 1.2 V versus NHE (brown) and reduction at −0.7 V vs NHE (red), **2** in acetonitrile upon spectroelectrochemical oxidation at 1.00 V versus NHE (dark blue) and reduction at −0.7 V vs NHE (light blue), and P3HT upon spectroelectrochemical oxidation at 1.0 V versus NHE (green).

2.1. Absorption Spectra. Steady state absorption spectra of thin films of P3HT, **1**, **2**, and PCBM are shown in Figure 2a. Films of **1** and **2** both absorb in the wavelength range below 500 nm. Additionally, **1** shows strong absorption ranging from 600 to 850 nm with the absorption peak at 753 nm while **2** absorbs from 600 to beyond 1050 nm with the absorption peak at 898 nm. The thiophene group as a replacement for the phenyl ring is responsible for the longer wavelength absorption of **2** in comparison with **1**.[41] The integration of **1** or **2** into P3HT:PCBM enhances therefore the light harvesting efficiency, especially in the near-IR absorption. Figure 2b shows the absorption spectra of thermally annealed P3HT:PCBM 1:1 wt % films and P3HT:PCBM films with different concentrations of **1** and **2**, respectively. To precisely access the changes of absorption profiles and intensities upon addition of **1** and **2**, similar thickness (ca. 100 nm) of the blend films were processed. The typical **1** and **2** absorption bands ranging from 650 to 800/900 nm increases steadily with increasing concentrations. Simultaneously, the absorption features of P3HT:PCBM decreases due to less content of P3HT, especially when the concentration of **1** is reaching 30 wt %. Interestingly, when turning to the **2** blended films, the decrease in the absorption region of P3HT is even more pronounced than in the **1** based blends even at **2** concentration of as low as 10 wt %. This evidence could be indicating that in **2** based ternary blends P3HT already has a lower degree of ordering as compared to **1** based ternary blends.[42−44]

All of the thermally annealed ternary blend films of P3HT:**1**/**2**:PCBM exhibited the distinguished shoulder peak around 600 nm, as shown in Figure 2b, suggesting that the crystallization of P3HT is not disturbed by the addition of **1** and **2** molecules.[44,45] The peak wavelengths of the **1** and **2** absorption were observed at around 746 nm for the **1** based ternary blends and at around 835 nm for the **2** based ternary blends when the concentration of dye molecules is below 30%. These bands were obviously red-shifted compared to the peak wavelengths of **1** and **2** dissolved in solutions (715 and 793 nm)[40] and blue-shifted compared to the peak wavelengths of **1** and **2** in thin films (753 and 898 nm, as shown in Figure 2a), suggesting that **1** and **2** do aggregate in ternary blends but not to the extent as in solution.[44] We further compared the relationship between the peak wavelength and the concentration of **1** and **2** molecules in the ternary blend films. As shown in Figure 2b, the absorption peak wavelengths of dye molecules in ternary films were red-shifted monotonically for **1** from 744 nm (10 wt % **1**) to 748 nm (30 wt % **1**) and for **2** from 834 nm (10 wt % **2**) to 836 nm (20 wt % **2**). Thus, these small but slight red-shifts observed for both ternary blend films are ascribable to an increase in the local concentration of dye molecules, probably due to a phase separation with crystallized P3HT regimes.

These results indicate that **1** and **2** molecules are located rather at the donor/acceptor interface after annealing of P3HT,[44] which is a key for improvement. However, it could not give a clear principle to guide the choice of what kind of dye molecule work as sensitizer. Thus, we determined detailedly the energy levels of both compounds as well as the optical features of their oxidized and reduced states by cyclic voltammetry and spectroelectrochemical characterization as described in the following section.

2.2. Cyclic Voltammetry and Spectroelectrochemical Characterization. HOMO and LUMO energy levels of **1** and **2** were estimated by cyclic voltammetry as shown in Figure 3a and have been calculated assuming that the HOMO level for the ferrocene/ferrocenium (Fc/Fc^+) standard is −4.78 eV with respect to vacuum.[46−48] In particular, the HOMO and LUMO energy levels of **1** were determined as −5.22 and −3.65 eV, respectively, and are located between the HOMO and LUMO levels of P3HT and PCBM (see Figure 1c).[46] Notably, **1** possesses sufficiently large band edge offsets relative to P3HT (0.12 eV relative to the HOMOs and 0.75 eV relative to the LUMOs) and relative to PCBM (0.78 eV the HOMOs and 0.65 eV the LUMOs), which suggests that excitons might energetically dissociate at P3HT:**1**, **1**:PCBM, and P3HT:PCBM interfaces. **2** shows a smaller bandgap (1.26 eV) compared to **1** (1.57 eV), and its HOMO energy level of −4.96 eV is higher than the HOMO energy level of P3HT (−5.10 eV), as depicted in Figure 1d. The energy values as derived by cyclic voltammetry would indicate that, for compound **2**, charge trapping should be more likely than exciton separation.

For the photoelectrochemical characterization, differential absorption spectra were recorded at potentials, where the one electron oxidation or the one electron reduction of **1** and **2** are expected.[40] In terms of electrochemical oxidation of **1**, just bleaching of the absorption band at 709 nm was observed. In contrast, the bleaching at 791 nm upon oxidation of **2** is accompanied by the growth of new bands at 391, 434, 472, and

dx.doi.org/10.1021/am400923b | ACS Appl. Mater. Interfaces 2013, 5, 5609−5616

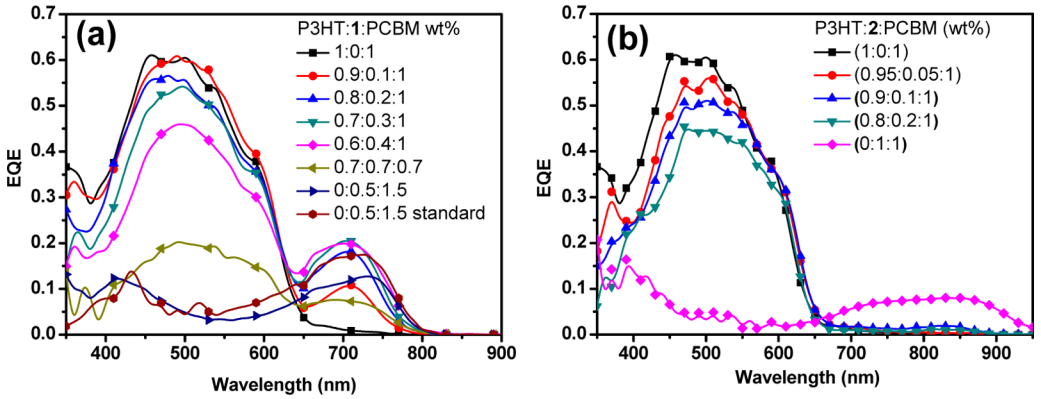

Figure 4. (a) EQE spectra of P3HT:**1**:PCBM and (b) of P3HT:**2**:PCBM with different relative concentrations of blend components.

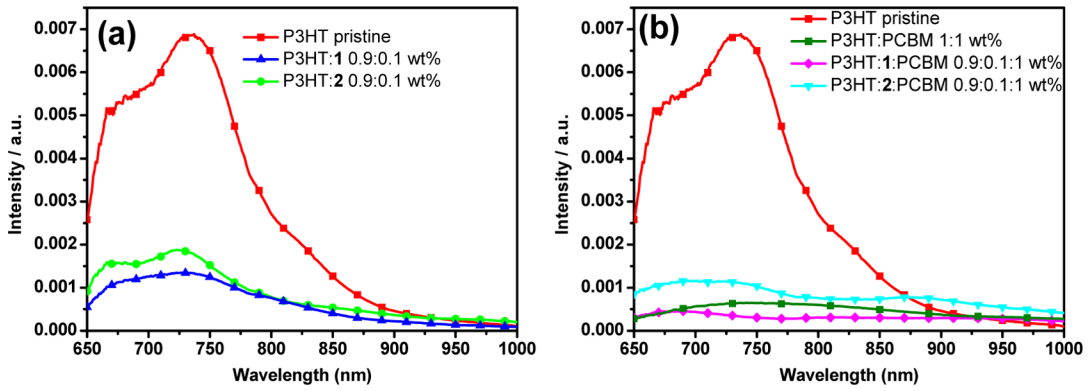

Figure 5. (a) Photoluminescence spectra of P3HT, P3HT:**1** 0.9:0.1 wt %, and P3HT:**2** 0.9:0.1 wt % and (b) P3HT, P3HT:PCBM 1:1 wt %, P3HT:**1**:PCBM 0.9:0.1:1 wt %, and P3HT:**2**:PCBM 0.9:0.1:1 wt % layers excited at 488 nm.

657 nm, which relates to the absorption features of **2** radical cation. A much higher extinction coefficient of cationic **2** in comparison with cationic **1** is accountable for the observed trend. Moreover, electrochemical reduction of **1** resulted in the depletion of the ground state absorption and the development of a series of bands at 463 and 492 nm. A similar trend was noted upon reduction of **2**, where the bleaching and the new feature are observed at 795 and 476 nm. Finally, electrochemical oxidation of P3HT reveals oxidation induced bleaching of the ground state absorption featuring distinct vibronic bands at 518 (0−2), 565 (0−1), and 615 nm (0−0) as well as new polaron absorption from 630 to 1100 nm.

2.3. Photovoltaic Properties. Glass/ITO/AZO/P3HT:**1**:PCBM/PEDOT:PSS/Ag and glass/ITO/AZO/P3HT: **2**:PCBM/PEDOT:PSS/Ag BHJ inverted configuration solar cells with different mixing ratios were fabricated and characterized. The *J*−*V* analysis of the reference as well as **1** and **2** blended devices is shown in Figure S1 and summarized in Table S1 in the Supporting Information. As expected, addition of **1** results in an increase of the short circuit current density. This increase in J_{sc} by addition of **1** results from extended absorption leading to a significant enhancement of photogenerated carriers in the near-IR (Figure 4a). Integrating the near-IR response from 650 to 800 nm suggests that the contribution of only 10% of **1** does result in a short circuit current density enhancement by approximately 10%. A further increase of **1** concentration results in enhanced near-IR photosensitization (see Figure 4a) up to approximately 30%. After that, the sensitization effect starts to level out and further increase of the **1** content does not further enhance the near-IR photocurrent generation. On the contrary, higher ratios of **1** (i.e., ≫ 20%) start to reduce the EQE contribution in the 500−600 nm regime, where P3HT is most sensitive, due to the relatively lower amount of P3HT in the ternary blend system. Simultaneously, the EQE in the **1** absorption region is not further improved because of its limited ability of direct charge generation, which is evident in the photoresponse spectrum **1**:PCBM device (as shown in Figure 4a).

A completely different trend is observed for **2** sensitized ternary blends. For P3HT:**2**:PCBM based devices, a continuous steady decrease of the photovoltaic performance with increasing concentration of **2** is recorded (as shown in Figure S1b and Table S1, Supporting Information). This suggests that light absorbed by **2** can not be extracted as photocurrent. On the contrary, even small additions of **2** reduce the photocurrent coming from P3HT absorption in the 500−600 nm region. The EQE spectra for P3HT:**2**:PCBM devices, presented in Figure 4b, prove that the EQE in the P3HT absorption (500−600 nm) decreases significantly while its contribution in the wavelength range of **2** absorption (700−900 nm) is negligible. This finding corroborates that **2** is not suitable as sensitizer.

To understand the origin of the photocurrent response upon the addition of **1** and **2**, photoluminescence and transient absorption spectroscopy experiments were carried out. These investigations target to unambiguously decide whether photoinduced charge transfer occurs in either composite.

2.4. Photoluminescence Spectroscopy (PL). Steady state emission spectra of the pristine (P3HT, **1**, and **2**) as well as blended (P3HT:PCBM 1:1 wt %, P3HT:**1** 0.9:0.1 wt %, P3HT:**2** 0.9:0.1 wt %, **1**:PCBM 0.9:0.1 wt %, P3HT:**1**:PCBM

0.9:0.1:1 wt %, and P3HT:**2**:PCBM 0.9:0.1:1 wt %) films (see Figure 5 and Figure S2, Supporting Information), taken at the excitation wavelengths of 488 and 630 nm were recorded to probe electronic communication within the blend components. As shown in Figure 5a,b, the PL of P3HT, excited at 488 nm, is quenched by more than 80% upon blending with 10 wt % of **1** and by 70% upon blending with 10 wt % of **2**. Compared with the PL spectra of P3HT:**1** 0.9:0.1 wt %, there is a significant IR-PL emission for the P3HT:**2** 0.9:0.1 wt % PL spectra, obviously coming from **2** via radiative or nonradiative energy transfer. Addition of 10% **2** into P3HT:PCBM increases the IR-PL by 80% relative to P3HT:PCBM. In summary, these findings are rather indicative for energy transfer between P3HT:**2** than for charge transfer.

In contrast, the PL of the P3HT:PCBM is further quenched by blending with 10 wt % of **1**. Further, the PL of pristine **1**, excited at 630 nm, is significantly quenched upon addition of 10 wt % of PCBM, suggesting charge transfer between **1** and PCBM (as shown in Figure S2, Supporting Information). Overall, the PL studies indicate charge transfer reactions between **1**, P3HT, and PCBM.

2.5. Transient Absorption Spectroscopy (TAS). To directly monitor the dynamics and fate of the photoexcited species in the blends, TAS of P3HT:**1**:PCBM 0.9:0.1:1 wt % and of P3HT:**2**:PCBM 0.9:0.1:1 wt %, upon laser excitation at 720 nm, was performed (see Figures 6 and S5, Supporting Information). Reference spectra of P3HT:PCBM 1:1 wt %, **1**, P3HT:**1** 1:1 wt %, **1**:PCBM 1:1 wt %, **2**, P3HT:**2** 1:1 wt %, and **2**:PCBM 1:1 wt % films were additionally recorded for comparison (see Figure S3, Supporting Information). In the blends, **1** and **2** were selectively excited as confirmed in control experiments with P3HT:PCBM 1:1 wt %, where no appreciable signals were observed (see Figure S3a, Supporting Information).

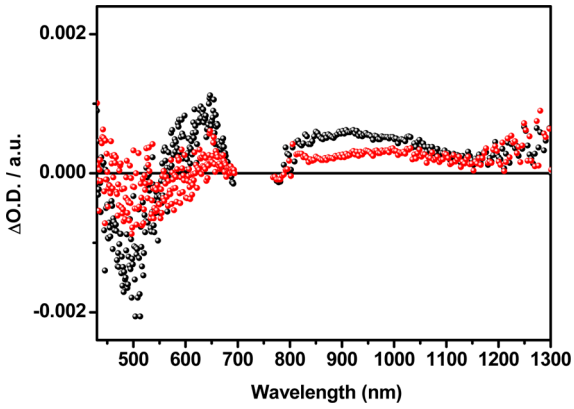

Figure 6. Transient absorption spectra of P3HT:**1**:PCBM 0.9:0.1:1 wt % film upon laser excitation at 720 nm at room temperature, recorded with time delays of 1 ps (black dots) and 7500 ps (red dots).

Photoexcitation of **1** at 720 nm gives rise in the differential absorption spectra to maxima at 530 and 1000 nm as well as a minimum at 723 nm, as shown in Figure S3b, Supporting Information. These maxima correlate to singlet−singlet transitions, while the minimum is due to the depletion of the ground state. In terms of decay kinetics, a long-lived component of around 1500 ps obtained from a multi-wavelength analysis ascribed to the singlet excited state lifetime of **1**. Additionally, a short-lived component that features a lifetime of ca. 70 ps is noted, which is assigned to an intermolecular charge transfer. To further corroborate the latter, transient absorption spectra of **1** and **2** were obtained in solution experiments following 720 nm excitation (see Figure S4, Supporting Information). In the corresponding experiments, the photoinduced absorption in the near-infrared region is missing owing to the lack of intermolecular charge transfer.

Figure S3c,d,f,g (Supporting Information) displays the differential absorption spectra following excitation of P3HT:**1** 1:1 wt %, **1**:PCBM 1:1 wt %, P3HT:**2** 1:1 wt %, and **2**:PCBM 1:1 wt % films. In comparison with the spectra of either **1** or P3HT:**1**, all of the spectra give rise to additional absorption maxima at 500 and 530 nm, which resemble the features similar to that of the **1** radical anion, implying an electron transfer process from P3HT to **1**. This process appears, however, to be nonquantitative, since some of the spectral features of P3HT polarons are superimposed by the bleaching of **1** and not discernible. In contrast, the spectra of P3HT:**2** are very similar to the spectra of just **2** and, in turn, charge transfer processes are unlikely to occur.

Notably, in the differential absorption spectra of **1**:PCBM, which was excited at 720 nm, a newly developing photoinduced absorption in the near-infrared, that is, a characteristic maximum at 1020 nm, relates to the generation of PCBM radical anions. Similarly, upon 720 nm excitation of **2**:PCBM, the differential absorption spectra reveal photoinduced absorption beyond 1000 nm, again owing to the formation of PCBM radical anions. In the visible region, a broad maximum that spans from 437 to 552 and a rather sharp maximum at 657 nm correlates well to the generation of the **2** radical cation. Overall, a likely rationale implies photoinduced electron transfer from both **1** and **2** to PCBM. Please note that this trend is consistent with the measured energy levels by CV and with SEC measurements.

Finally, P3HT:**1**:PCBM was probed at 720 nm. To this end, in the transient absorption spectra, photoinduced absorption between 600 and 700 nm ascribed to the P3HT delocalized polarons,[49] as a result of hole transfer from **1** to P3HT, is discernible. This finding was further corroborated by SEC measurements (see Figure 3). Additionally, a broad photoinduced absorption ranging from 780 to 1200 nm is recognizable. Taking the aforementioned into concern, photoexcited **1** is suitable to donate electrons to PCBM and holes to P3HT. These results suggested that **1** serves not only as a light-harvesting sensitizer but also as a funnel of charges owing to its appropriate energy levels for a charge transfer cascade. In contrast, differential absorption spectra of P3HT:**2**:PCBM, which was photexcited at 720 nm, failed to reveal any relevant signals upon near-IR sensitization. As a matter of fact, the low HOMO level of **2** is unsuitable to power a cascade hole transfer to P3HT (see Figure S5, Supporting Information). As a consequence, the **2** radical cation, generated by charge transfer to PCBM, is more likely to undergo geminate or nongeminate recombination, since hole transfer to P3HT is energetically unfavorable.

2.6. Atomic Force Microscopy (AFM). The macrostructure of the various films was investigated by AFM (Figure 7). The P3HT:PCBM, **1**:PCBM, and **2**:PCBM films (see Figure 7a,e,f) show surfaces with a root-mean-square (RMS) roughness of 1.79, 1.83, and 2.95 nm, respectively. The larger RMS of **2**:PCBM blend indicates a partial phase separation between **2** and PCBM. This is further corroborated by the fact that all other images of **2**:PCBM showed inhomogeneous films with large particles.

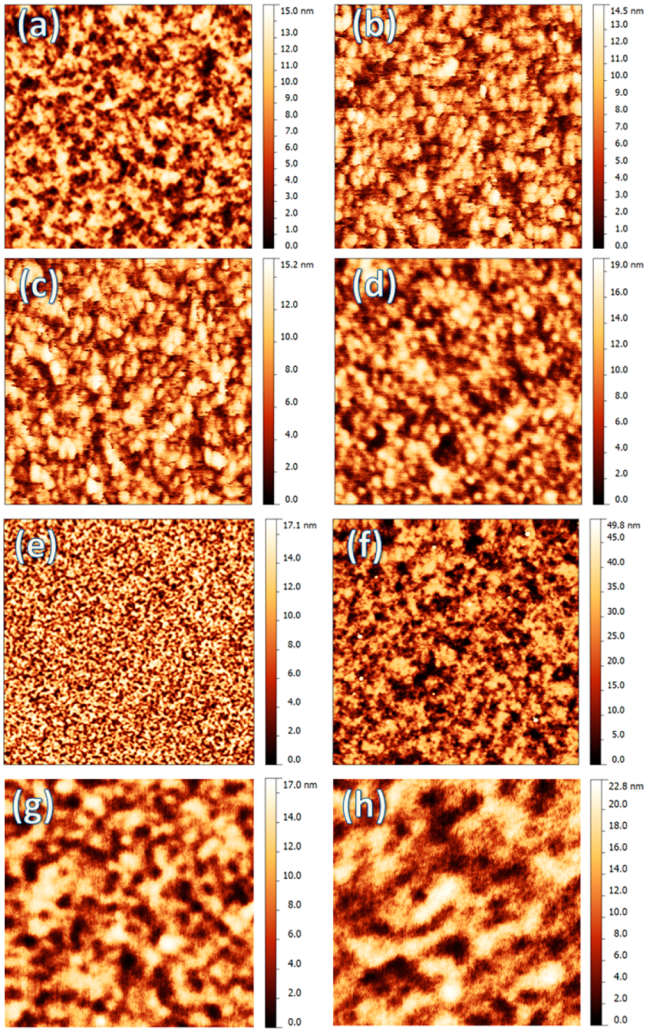

Figure 7. Contact mode AFM surface scans of thermally annealed films of (a) P3HT:PCBM 1:1 wt % (RMS = 1.79 nm), (b) P3HT:**1**:PCBM 0.9:0.1:1 wt % (RMS = 1.62 nm), (c) P3HT:**1**:PCBM 0.8:0.2:1 wt % (RMS = 1.69 nm), (d) P3HT:**1**:PCBM 0.7:0.7:0.7 wt % (RMS = 2.00 nm), (e) **1**:PCBM 1:3 wt % (RMS = 1.83 nm), (f) **2**:PCBM 1:1 wt % (RMS = 2.95 nm), (g) P3HT:**2**:PCBM 0.9:0.1:1 wt % (RMS = 2.01 nm), and (h) P3HT:**2**:PCBM 0.8:0.2:1 wt % (RMS = 2.36 nm). Surface area: 5 × 5 μm^2.

Notably, upon blending, 10 and 20 wt % **1** into the P3HT:PCBM matrix resulted in films with RMS roughnesses of 1.62 and 1.69 nm, respectively, and therefore did not result in significant morphology modifications (see Figure 7b,c). Further increasing the **1** concentration up to 50 wt % (see Figure 7d) results in larger RMS roughness of 2.00 nm, probably due to **1** aggregation. Finally, blending 10 and 20 wt % **2** into the P3HT:PCBM matrix (Figure 7g,h) disturbs the optimal phase segregation of P3HT:PCBM and further increases the RMS roughness (2.01 nm for 10 wt % **2**, 2.36 nm for 20 wt % **2**). Simultaneously, there is a trend for more separated phases, which is qualitatively in agreement with the results from absorption spectra and photoluminescence quenching.

3. CONCLUSION

In summary, we have investigated the photo sensitization mechanisms of two similar aza-BODIPY dyes when blended into P3HT:PCBM composites. Addition of up to 20% of **1** resulted in enhanced near-IR spectral photosensitivity of up to 20% as a result of near-IR sensitization and charge funneling. Higher concentrations of **1** did not result in stronger IR photocurrent contributions but rather decreased the charge generation efficiency of the P3HT:PCBM matrix. On the contrary, addition of **2** does not result in near-IR photocurrent sensitization, despite the fact that charge generation between **2** and PCBM is favored. With the HOMO level of **2** lying above the one of P3HT, charges are becoming trapped on **2** with no possibility of being transferred onto the P3HT matrix.

To avoid such undesired charge trapping, it is important that both the HOMO and the LUMO level of dye lie between those of P3HT and PCBM. Owing to the synthetic versatility of aza-BODIPY dyes, further energy levels and supramolecular structure tailoring is still possible. We believe that these findings provide an effective set of design rules for molecular sensitizers with enhanced performance.

4. EXPERIMENTAL SECTION

Absorption profiles were recorded with a Perkin-Elmer Lambda-35 absorption spectrometer from 350 to 1100 nm. CV measurements were performed with an Metrohm μ Autolab III/FRA2 potentiostat/galvanostat. A single-compartment, three-electrode cell configuration was used. A platinum foil with drop-casted polymer was utilized as the working electrode for P3HT, and glassy carbon was utilized as working electrode for **1** and **2**. A platinum wire served as the counter electrode, and a Ag wire was used as the quasi reference electrode. The supporting electrolyte was tetrabutylammonium hexafluorophosphate ($TBAPF_6$, electrochemical grade, Sigma-Aldrich), 0.1 M in anhydrous acetonitrile (Sigma-Aldrich). Scan rate was 10 mV/s^1. The potential was corrected against ferrocene/ferrocenium (Fc/Fc^+).

SEC experiments were performed with a home-built cell and a three-electrode setup. For P3HT, a drop-casted ITO slide was the working electrode. For **1** and **2** acetonitrile solutions, the working electrode was a platinum gauze. The counter electrode was a platinum wire, and a silver wire as quasi reference electrode was utilized. Potentials were applied and monitored with a MetrohmPGstat 101. The results are finally shown as differential spectra, that is, the difference between a spectrum with and without an applied potential. The spectra were recorded with a UV/vis/NIR spectrometer Cary 5000 (VARIAN).

PL data were collected using a Perkin−Elmer LS55 Fluorescence Spectrometer. Unless otherwise stated, the PL excitation wavelength was set to 488 nm (approximately the absorption maximum for P3HT) and 630 nm (around the absorption region for **1**).

For the TAS measurements, films and solutions were excited with a laser pulse (1 kHz, 150 fs pulse width, 100 nJ for films, 200 nJ for solutions) from an amplified Ti:Sapphire laser system (CPA 2101 Laser, Clark-MXR Inc.), and the excited states were probed with a second laser pulse that arrives at controllable times after the excitation pulse.

Single carrier devices were fabricated, and the dark current−voltage characteristics were measured and analyzed in the space charge limited (SCL) regime following ref 50. The structure of hole only devices was glass/ITO/PEDOT:PSS/active layer/PEDOT:PSS/Ag (100 nm). For the electron only devices, the structure was glass/ITO/AZO/active layer/Ca (15 m)/Ag (80 nm), where both Ca and Ag were evaporated. The reported mobility data are average values over the two cells of each sample at a given film composition. AFM measurements were performed with a Nanosurf Easy Scan 2 in contact mode.

Unless otherwise stated, the photovoltaic devices were fabricated in inverted architecture.The materials were deposited by doctor blading on indium tin oxide (ITO)-covered glass substrates (from Osram). These substrates were cleaned in water acetone and isopropyl alcohol before. After drying, the substrates were bladed with 50 nm Al-doped zinc oxide (AZO). Photovoltaic layers, consisting of P3HT (Merck Lisicon), **1**, and **2** (provided by M. Lorenz-Rothe), and the PCBM (Solenne) in 1:1 wt % ratios were dissolved at different concentrations in chlorobenzene (CB) and bladed on top of the AZO layer. The hole

dx.doi.org/10.1021/am400923b | ACS Appl. Mater. Interfaces 2013, 5, 5609−5616

transport layer of PEDOT:PSS (HC Starck, PEDOT PH) diluted in isopropyl was afterward directly doctor bladed on top of the active layer. The whole stack was thermally annealed on a hot plate at 140 °C for 5 min. Finally, a silver top electrode of 100 nm thickness was evaporated. The typical active area of the investigated devices was 10.4 mm^2. The current−voltage characteristics were measured using a source measurement unit from BoTest while the solar cells were illuminated under AM 1.5G irradiation on an OrielSol 1A Solar simulator (100 mW/cm^2). The EQE was detected with a lock-in amplifier under monochromatic illumination, which was calibrated with a monocrystalline silicon diode.

■ ASSOCIATED CONTENT

Ⓢ Supporting Information

Photovoltaic properties of devices, photoluminescence spectroscopy (PL), and transient absorption spectroscopy (TAS). This information is available free of charge via the Internet at http://pubs.acs.org.

■ AUTHOR INFORMATION

Corresponding Author

*E-mail: Min.Jie@ww.uni-erlangen.de.

Author Contributions

The manuscript was written through contributions of all authors. All authors have given approval to final version of the manuscript.

Notes

The authors declare no competing financial interest.

■ ACKNOWLEDGMENTS

The authors gratefully acknowledge the support of the Cluster of Excellence "Engineering of Advanced Materials" at the University of Erlangen-Nuremberg, which is funded by the German Research Foundation (DFG) within the framework of its "Excellence Initiative". This work has been funded by the DFG project, grant No. BR 4031/2-1, the Sonderforschungsbereich 953 "Synthetic Carbon Allotropes", the China Scholarship Council (CSC), and the BMBF project InnoProfile (grant No. 03IP602). We also thank the Solar Technologies go Hybrid (SolTech) and the "solar factory of the future" (Bavarian ministries of education and of economy) for financial support.

■ REFERENCES

(1) Günes, S.; Neugebauer, H.; Sariciftci, N. S. *Chem. Rev.* **2007**, *107*, 1324.
(2) Yu, G.; Gao, J.; Hummelen, J.; Wudl, C. F.; Heeger, A. J. *Science* **1995**, *270*, 1789.
(3) Thompson, B. C.; Fréchet, J. M. J. *Angew. Chem., Int. Ed.* **2008**, *47*, 58.
(4) Brabec, C. J.; Durrant, J. R. *MRS Bull.* **2008**, *33*, 670.
(5) Li, Y. F.; Zou, Y. P. *Adv. Mater.* **2008**, *20*, 2952.
(6) He, Z.; Zhong, C.; Su, S.; Xu, M.; Wu, H.; Cao, Y. *Nat. Photonics* **2012**, *6*, 593.
(7) Green, M. A.; Emery, K.; Hishikawa, Y.; Warta, W.; Dunlop, E. D. *Prog. Photovoltaics: Res. Appl.* **2012**, *20*, 12.
(8) Dang, M. T.; Hirsch, L.; Wantz, G. *Adv. Mater.* **2011**, *23*, 3597.
(9) Hou, J. H.; Tan, Z. A.; Yan, Y.; He, Y. J.; Yang, C. H.; Li, Y. F. *J. Am. Chem. Soc.* **2006**, *128*, 4911.
(10) Koster, L. J. A.; Mihailetchi, V. D.; Blom, P. W. M. *Appl. Phys. Lett.* **2006**, *88*, 093511.
(11) Ross, R. B.; Cardona, C. M.; Guldi, D. M.; Sankaranarayanan, S. G.; Reese, M. O.; Kopidakis, N.; Peet, J.; Walker, B.; Bazan, G. C.; Van Keuren, E.; Holloway, B. C.; Drees, M. *Nat. Mater.* **2009**, *8*, 208.
(12) Ross, R. B.; Cardona, C. M.; Swain, F. B.; Guldi, D. M.; Sankaranarayanan, S. G.; Van Keuren, E.; Holloway, B. C.; Drees, M. *Adv. Funct. Mater.* **2009**, *19*, 2332.
(13) He, Y.; Chen, H. Y.; Hou, J.; Li, Y. *J. Am. Chem. Soc.* **2010**, *132*, 1377.
(14) Peet, J.; Kim, J. Y.; Coates, N. E.; Ma, W. L.; Moses, D.; Heeger, A. J.; Bazan, G. C. *Nat. Mater.* **2007**, *6*, 497.
(15) Hou, J.; Chen, H. Y.; Zhang, S.; Li, G.; Yang, Y. *J. Am. Chem. Soc.* **2008**, *130*, 16144.
(16) Huang, F.; Chen, K. S.; Yip, H. L.; Hau, S. K.; Acton, O.; Zhang, Y.; Lou, J.; Jen, A. K. Y. *J. Am. Chem. Soc.* **2009**, *131*, 13886.
(17) Min, J.; Zhang, Z. G.; Zhang, S. Y.; Li, Y. F. *Chem. Mater.* **2012**, *24*, 3247.
(18) Li, Y. F. *Acc. Chem. Res.* **2012**, *45*, 723.
(19) Huo, L. J.; Zhang, S. Q.; Guo, X.; Xu, F.; Li, Y. F.; Hou, J. H. *Angew. Chem., Int. Ed.* **2011**, *50*, 9697.
(20) Chen, H.-C.; Chen, Y.-H.; Liu, C.-C.; Chien, Y.-C.; Chou, S.-W.; Chou, P.-T. *Chem. Mater.* **2012**, *24*, 4766.
(21) Wang, H. Q.; Stubhan, T.; Osvet, A.; Litzov, I.; Brabec, C. J. *Sol. Energy Mater. Sol. Cells* **2012**, *105*, 196.
(22) Kim, J. Y.; Lee, K.; Coates, N. E.; Moses, D.; Nguyen, T. Q.; Dante, M.; Heeger, A. J. *Science* **2007**, *317*, 222.
(23) Gevaerts, V. S.; Furlan, A.; Wienk, M. M.; Turbiez, M.; Janssen, R. A. J. *Adv. Mater.* **2012**, *24*, 2130.
(24) Dennler, G.; Prall, H. J.; Koeppe, R.; Egginger, M.; Autengruber, R.; Sariciftci, N. S. *Appl. Phys. Lett.* **2006**, *89*, 073502.
(25) Ameri, T.; Dennler, G.; Lungenschmied, C.; Brabec, C. *J. Energy Environ. Sci.* **2009**, *2*, 347.
(26) Rauch, T.; Böberl, M.; Tedde, S. F.; Fürst, J.; Kovalenko, M. V.; Hesser, G.; Lemmer, U.; Heiss, W.; Hayden, O. *Nat. Photonics* **2009**, *3*, 332.
(27) Cate, S. T.; Schins, J. M.; Siebbeles, L. D. A. *ACS Nano* **2012**, *6*, 8983.
(28) Ameri, T.; Min, J.; Li, N.; Machui, F.; Baran, D.; Forster, M.; Schottler, K. J.; Dolfen, D.; Scherf, U.; Brabec, C. J. *Adv. Energy Mater.* **2012**, *2*, 1198.
(29) Koppe, M.; Egelhaaf, H. J.; Dennler, G.; Scharber, M. C.; Brabec, C. J.; Schilinsky, P.; Hoth, C. N. *Adv. Funct. Mater.* **2010**, *20*, 338.
(30) Chen, M. C.; Liaw, D. J.; Huang, Y. C.; Wu, H. Y.; Tai, Y. *Sol. Energy Mater. Sol. Cells* **2011**, *95*, 2621.
(31) Honda, S.; Nogami, T.; Ohkita, H.; Benten, H.; Ito, S. *ACS Appl. Mater. Interfaces* **2009**, *1*, 804.
(32) Huang, J. H.; Velusamy, M.; Ho, K. C.; Lin, J. T.; Chu, C. W. *J. Mater. Chem.* **2010**, *20*, 2820.
(33) Kubo, Y.; Watanabe, K.; Nishiyabu, R.; Hata, R.; Murakami, A.; Shoda, T.; Ota, H. *Org. Lett.* **2011**, *13*, 4574.
(34) Tasior, M.; O'Shea, D. F. *Bioconjugate Chem.* **2010**, *21*, 1130.
(35) Hong, Z. R.; Lessmann, R.; Maennig, B.; Huang, Q.; Harada, K.; Riede, M.; Leo, K. *J. Appl. Phys.* **2009**, *106*, 064511.
(36) Rousseau, T.; Cravino, A.; Bura, T.; Ulrich, G.; Ziessel, R.; Roncali, J. *J. Mater. Chem.* **2009**, *19*, 2298.
(37) Kim, B.; Ma, B.; Donuru, V. R.; Liu, H.; Frechet, J. M. J. *Chem. Commun.* **2010**, *46*, 4148.
(38) Rousseau, T.; Cravino, A.; Ripaud, E.; Leriche, P.; Rihn, S.; De Nicola, A.; Ziessel, R.; Roncali, J. *Chem. Commun.* **2010**, *46*, 5082.
(39) Mueller, T.; Gresser, R.; Leo, K.; Riede, M. *Sol. Energy Mater. Sol. Cells* **2012**, *99*, 176.
(40) Gresser, R.; Hummert, M.; Hartmann, H.; Leo, K.; Riede, M. *Chem.—Eur. J.* **2011**, *17*, 2939.
(41) Zhang, X.; Yu, H.; Xiao, Y. *J. Org. Chem.* **2012**, *77*, 669.
(42) Li, G.; Shrotriya, V.; Huang, J. S.; Yao, Y.; Moriarty, T.; Emery, K.; Yang, Y. *Nat. Mater.* **2005**, *4*, 864.
(43) Chen, D. A.; Nakahara, A.; Wei, D. G.; Nordlund, D.; Russell, T. P. *Nano Lett.* **2011**, *11*, 561.
(44) Honda, S.; Ohkita, H.; Benten, H.; Ito, S. *Adv. Energy Mater.* **2011**, *1*, 588.
(45) Jiang, X.; Osterbacka, R.; Korovyanko, O.; An, C. P.; Horowitz, B.; Janssen, R. A. J.; Vardeny, Z. V. *Adv. Funct. Mater.* **2002**, *12*, 587.

(46) Cardona, C. M.; Li, W.; Kaifer, A. E.; Stockdale, D.; Bazan, G. C. *Adv. Mater.* **2011**, *23*, 2367.
(47) He, Y. J.; Li, Y. F. *Phys. Chem. Chem. Phys.* **2011**, *13*, 1970.
(48) He, Y. J.; Zhao, G. J.; Peng, B.; Li, Y. F. *Adv. Funct. Mater.* **2010**, *20*, 3383.
(49) Zhang, W.; Hu, R.; Li, D.; Huo, M. M.; Ai, X. C.; Zhang, J. P. *J. Phys. Chem. C* **2012**, *116*, 4298.
(50) Azimi, H.; Senes, A.; Scharber, M. C.; Hingerl, K.; Brabec, C. J. *Adv. Energy Mater.* **2011**, *1*, 1162.